Semnan University

Progress in Physics of Applied Materials

journal homepage: https://ppam.semnan.ac.ir/

Doped t-J model of twisted bilayer WSe_2

Mohammad-Hossein Zare[1]*, Hamid Mosadeq[2]

[1] *Department of Physics, Qom University of Technology, Qom, Iran*
[2] *Department of Physics, Faculty of Science, Shahrekord University, Shahrekord, Iran*

ARTICLE INFO

Article history:
Received: 26 November 2023
Revised: 10 December 2023
Accepted: 16 December 2023

Keywords:
Generalized Kane-Mele model
Mean-field theory
Unconventional superconductivity
Mixing pairing

ABSTRACT

Experiments in twisted materials have shown evidence of exotic phases, such as correlated insulating phases and unconventional superconductivity states. Recently, the topological moiré valance bands with opposite Chern numbers in twisted bilayer WSe_2 have been described with a generalized Kane-Mele model on a honeycomb lattice. Interaction strength, band filling, and bandwidth of twisted materials are well controlled employing varying the twist angle and using three-dimensional dielectric environments. To describe the existence of these exotic phases in the twisted bilayer WSe_2, we consider the doped moiré Hubbard model in the strongly correlated limit. Here, we are interested in studying the stability of different superconductivity channels by employing the mean-filed theory. We find that the admixture of the nearest-neighbor-$d + id$- and next-nearest-neighbor-$es + f$-wave pairings is the superconducting ground state at any doping level. In addition, the obtained results show that the quasi-spin-orbit interaction plays an essential role in the stability of this mixed singlet-triplet superconductivity.

1. Introduction

Twisted bilayer systems consisting of semiconductors or semimetals with different lattice constants or orientations of the individual layers form in van der Waals bilayers [1-4]. Recent experimental observations have proven the existence of the electron current without resistance in twisted bilayer graphene with voltage gating in the magic angles of about 1 - 1.5° [5,6]. Due to its central importance for fundamental physics, the electronic structure of the sandwich of two-layer graphene has attracted much interest [7-21]. Theoretical studies have shown the existence of the nearly flat bands that are separated from other bands with a large gap [9]. As a result, the interaction effects can increase when the chemical potential lies in these nearly flat bands via the carrier density. The Mott insulator behavior for the twisted-bilayer graphene was experimentally shown for filling 1/4 or 3/4 at low temperatures [5]. Inducing the carrier charges via the voltage gate gives rise to a superconductivity phase in the twisted-bilayer graphene at low temperatures [6]. It should be noted that the inducing superconductivity phase is predicted to be unconventional [22-27]. At present, these new findings can help the understanding of unconventional superconductivity at room temperature and the study of strongly correlated systems [28-32].

Apart from the twisted bilayer graphene, theoretical [33,34] and experimental [35,36] studies have verified the existence of the flat bands in the twisted bilayer transition metal dichalcogenides (TMD), which are composed of two similar semiconductors. In contrast to the twisted bilayer graphene, in which the flat bands are formed only within a narrow range (±0.1°) around the magic angle 1.1°, in TMDs the flat bands appear in larger windows of twist angles in the twisted TMD homobilayer. More recently, experimental observations have reported the discovery of strongly correlated insulating phases and superconductivity for this class of materials [35,36]. Mott insulating behavior originates from the flat bands because the Coulomb potential dominates the kinetic energy of the band electrons.

In this paper, we are interested in investigating the superconducting gap symmetry that is the fundamental

* Corresponding author. Tel.: +98 2536169000
E-mail address: zare@qut.ac.ir

Cite this article as:
Zare M.H., Mosadeq H., 2023. Doped t-J model of twisted bilayer WSe_2. *Progress in Physics of Applied Materials*, 3(2), pp. 125-130.
DOI: **10.22075/PPAM.2023.32414.1070**

property of the superconducting state in this material by applying a mean-field approach. For this purpose, we study the competition of spin-singlet superconductivity and spin-triplet superconductivity in the hole-doped moiré Hubbard model on a honeycomb lattice in the strongly correlated limit. The importance of studying the twisted TMD bilayers is due to the fact that the strength of the spin-orbit interaction in these systems can be controlled by the interlayer potential difference [37]. By changing the interlayer potential difference, we can manipulate the band structure of the twisted TMD homobilayer so that Van Hove singularities appear in the density of states, which results in easy control of the spin-orbit coupling.

2. Model Hamiltonian

Recently, the effective two-orbital model on a honeycomb lattice is proposed for the twisted WSe_2/WSe_2 homobilayers with small twist angles near 0° as follows [34]:

$$H_k = t_1 \sum_{\langle ij\rangle,\alpha} c^{\dagger}_{i,\alpha} c_{j,\alpha} + t_2 \sum_{\langle\langle ij\rangle\rangle,\alpha} e^{\frac{2\pi i}{3}\nu_{ij}} c^{\dagger}_{i,\alpha} c_{j,\alpha} \qquad (1)$$

where $c^{\dagger}_{i\alpha}$ ($c_{i\alpha}$) stands for the creation (annihilation) operator of an electron with spin-up and spin-down $\alpha = \pm$ on site i. The first term represents the nearest-neighbor (NN) hopping with amplitude t_1, and the second term denotes the bond and spin-dependent hopping between the next-nearest-neighbor (NNN) on a honeycomb lattice which $\nu_{ij} = (\widehat{d_1} \times \widehat{d_2})_z$. Note that the unit vectors $\widehat{d_1}$ and $\widehat{d_2}$ are the vectors connecting the next-nearest neighbors. In this paper, we set $t_1 = 0.29$ meV and $t_2 = 0.06$ meV [34]. In Figure 1, we indicate the two valence bands have been obtained from the effective in Eq. (1). Since the kinetic energy is strongly decreased under the suppressed bandwidth condition in the moiré bands, thus many-body effects for electrons in the flat bands are remarkably increased. The ration of interaction strength to bandwidth of moiré homobilayers is well modified through varying the twist angle and using a three-dimensional environment. Figures 2(c)-(d) show the evolution of the Fermi surface with respect to chemical potential $\mu = -0.2, -0.4$, respectively. For the hole-doped for $\mu = -0.2$, the Fermi surface has electron-like pocket centered around the K points of the Brillouin zone (BZ). At $\mu = -0.23$, the contours of the Fermi surface touch the borders of the BZ at the M points. This filling marks a Lifshitz transition, which results in a van Hove singularity in the density of state and a changing of the topology of the Fermi surface. At $\mu = -0.23$, the topology of the Fermi surface has been changed into hole-like textures, with pockets, which are centered around the Γ points.

Adding electron-electron interaction to the above Hamiltonian, Eq. (1), by an on-site repulsive Hubbard term:

$$H_U = U \sum_i n_{i\uparrow} n_{i\downarrow} \qquad (2)$$

gives quasi Kane-Mele-Hubbard model. Here, $n_{i\alpha} = c^{\dagger}_{i\alpha} c_{i\alpha}$ is a number operator, and U is on-site Coulomb interaction. When the on-site Coulomb repulsion U is much larger than the hopping integrals t_1 and t_2, the charge fluctuations are squeezed, and one can project the half-filled Hamiltonian to the lowest Hubbard subband for which the condition of the single-occupied site is fulfilled. This procedure can be done perturbatively in terms of the ratios t_1/U and t_2/U. Two-second order, we find an effective spin Hamiltonian [38] similar to the Kane-Mele Heisenberg model [39] as follows:

$$H_J = \sum_{\langle ij\rangle} J_1 \boldsymbol{S}_i \cdot \boldsymbol{S}_j + \sum_{\langle\langle ij\rangle\rangle} [J_2 \boldsymbol{S}_i \cdot \boldsymbol{S}_j - g_2\left(S_i^x S_j^x + S_i^y S_j^y - S_i^z S_j^z\right) - \nu_{ij} \boldsymbol{D} \cdot (\boldsymbol{S}_i \times \boldsymbol{S}_j)] \qquad (3)$$

This effective spin Hamiltonian consists of antiferromagnetic Heisenberg exchange interactions between nearest-neighbor and next-nearest-neighbor with $J_1 = 4t_1^2/U$, $J_2 = t_2^2/U$, and $g_2 = 3J_2$, respectively. In addition, from the spin- and bond-dependent hopping integral term between NN neighbors, we obtain the XY term that favors in-plane ferromagnetic order; the Ising term which favors antiparallel of spins out-of-plane and the antisymmetric Dzyaloshinskii-Moriya (DM) exchange with $D = 2\sqrt{3}J_2\hat{z}$. The DM interaction is an asymmetric exchange interaction coupling that favors a noncollinear orientation of spins. As a result, the noncollinear orientation of spins leads to the stability of triplet-pairing correlation.

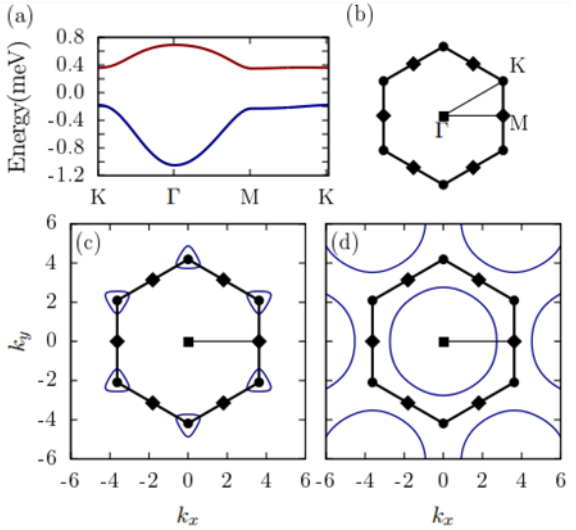

Fig.1. (a) Moiré band structure of twisted TMD homobilayer obtained by suing the effective tight-binding model in Eq. (1), where the hopping integral parameters were set as $t_1 = 0.29$ meV and $t_2 = 0.06$ meV [34]. (b) The first BZ and the high-symmetry points of the honeycomb lattice. Fermi surface of twisted TMD homobilayer for (c)$\mu = -0.2$ and (d)$\mu = -0.4$.

3. Method and Results

To investigate the potential superconducting pairing symmetry in the hole-doped homobilayer moiré systems, we start from the $t-J$ model as $H_{KJ} = H_K + H_J$. For this purpose, it is necessary to replace the spin operators in H_J with fermions. For this end, we utilize the auxiliary fermions as $\mathbf{S}_i = \frac{1}{2} f^{\dagger}_{i,\alpha} \boldsymbol{\sigma}_{\alpha,\beta} f_{j,\beta}$ in which $f^{\dagger}_{i,\alpha}(f_{i,\alpha})$ is the fermionic spinon creation (annihilation) operator on site i.

Since the effective Hamiltonian Eq. (3) includes the exchange interactions between nearest-neighbor and next-nearest-neighbor on the honeycomb lattice, therefore we define the related spin-singlet- and spin-triplet as follows:

$$s_{ij} = \frac{i}{\sqrt{2}}\sum_{\alpha,\beta}(\sigma_y\sigma_0)_{\alpha,\beta} f_{i,\alpha} f_{j,\beta},$$
$$t^{\rho}_{ij} = \frac{i}{\sqrt{2}}\sum_{\alpha,\beta}(\sigma_\rho\sigma_y)_{\alpha,\beta} f_{i,\alpha} f_{j,\beta} \quad (4)$$

in which i and j standing for nearest-neighbors and next-nearest neighbors on the honeycomb lattice. The index $\rho = x, y, z$ identifies three triplet components and $\sigma = (\sigma_x, \sigma_y, \sigma_z)$ are the Pauli matrices in the spin space, and σ_0 is the 2×2 identity matrix. The effective Hamiltonian can easily be re-expressed in terms of the spin-singlet and spin-triplet pairing as follows:

$$H_J = -\sum_{\langle ij\rangle} J_1\ s^{\dagger}_{ij} s_{ij} - \sum_{\langle\langle ij\rangle\rangle}[J_2\ s^{\dagger}_{ij} s_{ij} + g_2\ t^{z\dagger}_{ij} t^{z}_{ij} + \frac{i}{2}\nu_{ij} D(s^{\dagger}_{ij} t^{z}_{ij} - t^{z\dagger}_{ij} s_{ij})] + H.c., \quad (5)$$

where the constant terms have been dropped because they only shift the overall energy. The interaction Hamiltonian, Eq. (5), in the mean-field approximation rewritten in terms of the nearest-neighbor spin-singlet MF order parameter, the next nearest-neighbor spin-singlet and spin-triplet MF order parameters as follows:

$$\psi_{\hat{\delta}_i} = < s_{ij} > /\sqrt{2},$$
$$\psi_{\hat{\delta}'_i} = < s_{ij} > /\sqrt{2},$$
$$\psi'^{\rho}_{\hat{\delta}'_i} = < t^{\rho}_{ij,\delta'} > /\sqrt{2} \quad (6)$$

which the indices $\hat{\delta}_i$ and $\hat{\delta}'_i$ indicate the direction of the nearest-neighbor and next-nearest-neighbor of ith on honeycomb lattice site. Using these definitions, we now obtain the mean-field Hamiltonian reads as:

$$H_{MF} = H_k - \sum_{\langle ij\rangle} J_1\ \psi_{ij} s^{\dagger}_{ij} - \sum_{\langle\langle ij\rangle\rangle}[(J_2\ \psi'_{ij} + \frac{i}{2} D\nu_{ij} d'^{z}_{ij}) s^{\dagger}_{ij} + (g_2\ d'^{z}_{ij} - \frac{i}{2} D\nu_{ij}\psi'_{ij}) t^{z\dagger}_{ij}] - \mu\sum_{i,\alpha} f^{\dagger}_{i,\alpha} f_{i,\alpha} + H.c. \quad (7)$$

To ensure the Gutzwiller projection .e.g. to abandon from double counting of interparticle interaction, we utilize the so-called $U(1)$ slave boson theory in which the bare hopping integrals t_1 and t_2 in the kinetic term, H_K, rescaled with δ [40,41]. The order parameters in Eq. (7) are obtained via the self-consistent equations as:

$$\psi = -\frac{J_1}{\sqrt{2}}(\langle s_{i\delta_1}\rangle, \langle s_{i\delta_2}\rangle, \langle s_{i\delta_3}\rangle) \quad (8)$$
$$\psi' = -\frac{1}{\sqrt{2}}(J_2\langle s_{i\delta'_1}\rangle + \frac{i}{2} D\nu_{i\delta'_1}\langle t^{z}_{i\delta'_1}\rangle,$$
$$J_2\langle s_{i\delta'_2}\rangle + \frac{i}{2} D\nu_{i\delta'_2}\langle t^{z}_{i\delta'_2}\rangle,$$
$$J_2\langle s_{i\delta'_3}\rangle + \frac{i}{2} D\nu_{i\delta'_3}\langle t^{z}_{i\delta'_3}\rangle)$$
$$d'^{z} = -\frac{1}{\sqrt{2}}(g_2\langle t^{z}_{i\delta'_1}\rangle - \frac{i}{2} D\nu_{i\delta'_1}\langle s_{i\delta'_1}\rangle,$$
$$g_2\langle t^{z}_{i\delta'_2}\rangle - \frac{i}{2} D\nu_{i\delta'_2}\langle s_{i\delta'_2}\rangle,\ g_2\langle t^{z}_{i\delta'_3}\rangle - \frac{i}{2} D\nu_{i\delta'_3}\langle s_{i\delta'_3}\rangle).$$

As is clear, the Heisenberg exchange interactions J_1 and J_2 lead to the producing of the singlet pairing on the nearest and next-nearest-neighbors, respectively. The Kane-Mele term generates the equal spin triplet-paring with $m_z = 0$, and the DM term mixes the singlet and triplet channels on the next-nearest neighbors of the honeycomb lattice, respectively. We now go the momentum space using transformations

$$f_{i,l,\alpha} = \frac{1}{\sqrt{N}}\sum_{\boldsymbol{q}} e^{i\boldsymbol{q}\cdot\boldsymbol{R}} f_{\boldsymbol{q},l,\alpha} \quad (9)$$

here R goes through the different unit cells, s denotes the sublattice index. By also including the chemical potential, we obtain a Bogoliubov-de Gennes (BdG) Hamiltonian on honeycomb lattice with two sublattices ($l = 1,2$) in two-dimensional (2D) which can be written as

$$H = \frac{1}{2}\sum_{\mathbf{q}} \Phi^{\dagger}_{\mathbf{q}} M_{\mathbf{k}} \Phi_{\mathbf{q}}$$

with $\Phi_{\mathbf{q}} = (f^{\dagger}_{\mathbf{q},l,\uparrow}, f^{\dagger}_{\mathbf{q},l,\downarrow}, f_{-\mathbf{q},l,\uparrow}, f_{-\mathbf{q},l,\downarrow})$

and the 8×8 matrix:

$$M_{\boldsymbol{k}} = \begin{pmatrix} \xi(\boldsymbol{q}) & \Delta(\boldsymbol{q}) \\ \Delta^{\dagger}(\boldsymbol{q}) & -\xi^{*}(-\boldsymbol{q}) \end{pmatrix}$$

Where

$$\xi(\boldsymbol{q}) = t_1(\boldsymbol{q}) \otimes \sigma_0 + (t_2(\boldsymbol{q}) - \mu)\sigma_0 - t'_2(\boldsymbol{q})\sigma_z \otimes \sigma_z, \quad (10)$$

with

$$t_1(\mathbf{q}) = \begin{pmatrix} 0 & \gamma(\mathbf{q}) \\ \gamma^{*}(\mathbf{q}) & 0 \end{pmatrix},$$
$$\gamma(\mathbf{q}) = t_1(e^{-\mathrm{i}\frac{q_x}{\sqrt{3}}} + e^{\frac{\mathrm{i}}{2}(\frac{q_x}{\sqrt{3}} - q_y)} + e^{\frac{\mathrm{i}}{2}(\frac{q_x}{\sqrt{3}} + q_y)}),$$
$$t_2(\boldsymbol{q}) = -t_2(cos(q_y) + cos(\frac{\sqrt{3}}{2}q_x - \frac{1}{2}q_y) + cos(\frac{\sqrt{3}}{2}q_x + \frac{1}{2}q_y))$$
$$t'_2(\boldsymbol{q}) = \sqrt{3}t_2(sin(q_y) + sin(\frac{\sqrt{3}}{2}q_x - \frac{1}{2}q_y) - sin(\frac{\sqrt{3}}{2}q_x + \frac{1}{2}q_y)), \quad (11)$$

and the superconducting gap function is given by:

$$\Delta(\boldsymbol{q}) = \sigma_x \otimes \Delta_1(\boldsymbol{q}) + i\sigma_y \otimes \Delta_2(\boldsymbol{q}), \quad (12)$$
$$\Delta_1(\mathbf{q}) = \begin{pmatrix} d_1(\mathbf{q}) + d_2(\mathbf{q}) & 0 \\ 0 & -d_1(\mathbf{q}) + d_2(\mathbf{q}) \end{pmatrix},$$
$$\Delta_2(\boldsymbol{q}) = \begin{pmatrix} d_3(\boldsymbol{q}) + d_4(\boldsymbol{q}) & d_5(\boldsymbol{q}) \\ d_5(-\boldsymbol{q}) & d_3(\boldsymbol{q}) - d_4(\boldsymbol{q}) \end{pmatrix}$$

In which

$$d_1(\boldsymbol{q}) = D(-\psi'_{\delta'_1} sin(-q_y) + \psi'_{\delta'_2} sin(\frac{\sqrt{3}}{2}q_x - \frac{1}{2}q_y) - \psi'_{\delta'_3} sin(\frac{\sqrt{3}}{2}q_x + \frac{1}{2}q_y)),$$

$$d_2(\mathbf{q}) = 2ig_2\Big(d^z_{\delta'_1}\sin(-q_y) + d^z_{\delta'_2}\sin(\frac{\sqrt{3}}{2}q_x - \frac{1}{2}q_y) + d^z_{\delta'_3}\sin(\frac{\sqrt{3}}{2}q_x + \frac{1}{2}q_y)\Big),$$

$$d_3(\boldsymbol{q}) = 2J_2(\psi'_{\delta'_1} cos(-q_y) + \psi'_{\delta'_2} cos(\frac{\sqrt{3}}{2}q_x - \frac{1}{2}q_y) + \psi'_{\delta'_3} cos(\frac{\sqrt{3}}{2}q_x + \frac{1}{2}q_y)),$$

$$d_4(\mathbf{q}) = iD\Big(-d^z_{\delta'_1}\cos(-q_y) + d^z_{\delta'_2}\cos(\frac{\sqrt{3}}{2}q_x - \frac{1}{2}q_y) - d^z_{\delta'_3}\cos(\frac{\sqrt{3}}{2}q_x + \frac{1}{2}q_y)\Big),$$

$$d_5(\boldsymbol{q}) = J_1(\psi_{\delta_1}e^{-i\frac{q_x}{\sqrt{3}}} + \psi_{\delta_2}e^{i(\frac{q_x}{2\sqrt{3}} - \frac{q_y}{2})} + \psi_{\delta_3}e^{i(\frac{q_x}{2\sqrt{3}} + \frac{q_y}{2})}), \quad (13)$$

To diagonalize the kinetic Hamiltonian (10), we obtain eigenvalues as:

$$\xi_{1,2}(\boldsymbol{q}) = t_2(\boldsymbol{q}) - \mu \pm \sqrt{t'^2_2(\boldsymbol{q}) + |g(\boldsymbol{q})|^2}, \quad (14)$$

Let the expectation value for the number of electrons per lattice site be $1-\delta$. Then

$$\delta = \frac{1}{2N}\sum_q [tanh(\beta_c\xi_1/2) + tanh(\beta_c\xi_2/2)], \quad (15)$$

The dependence of the doping on the chemical potential is shown in Figure 2 at two different temperatures. Here, δquantifies the hole doping so that $1-\delta$ is the average number of electrons per site.

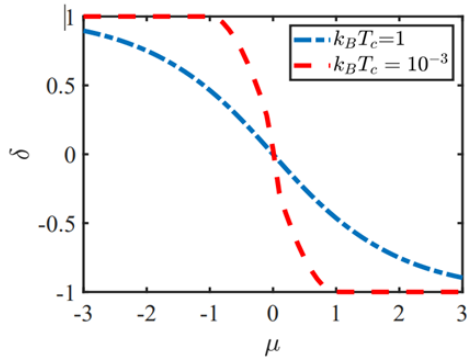

Fig.2. The dependence of the doping level δ on the chemical potential.

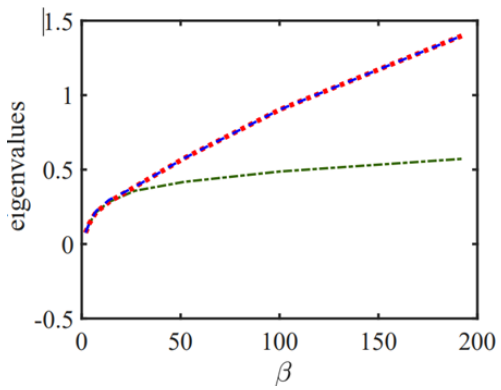

Fig.3. Possible solutions of the linear gap equations in Eq. (17) for the singlet case with $J_2 = D = 0$.

Close to the critical temperature of the superconducting phase transition, the order parameters are suppressed and we can obtain linearized gap equations [42]. In the absence of the NN neighbor hopping ($t_2 = 0$), we can write the gap equations as

$$\vec{\Delta} = \vec{M}(\beta_c)\vec{\Delta}, \quad (16)$$

where $\vec{\Delta} = (\Delta_x, \Delta_y, \Delta_z)^{\dagger}$and

$$\vec{M} = J_1\begin{pmatrix} D & B & B \\ B & D & B \\ B & B & D \end{pmatrix}$$

the elements of matrices D and B are given by

$$D(\beta_c,\mu) = \frac{1}{2N}\sum_q\{[\frac{tanh(\beta_c\xi_1/2)}{2\xi_1} + \frac{tanh(\beta_c\xi_2/2)}{2\xi_2}] cos(q.\delta_i)\, cos(q.\delta_i - \varphi_\delta) + \frac{sinh(\beta_c\mu)}{2\,cosh(\beta_c\xi_1/2)\,cosh(\beta_c\xi_2/2)} sin(q.\delta_i)\, sin(q.\delta_i - \varphi_\delta)\}$$

for all $i = x, y, z$. Similarly

$$B(\beta_c,\mu) = \frac{1}{2N}\sum_q\{[\frac{tanh(\beta_c\xi_1/2)}{2\xi_1} + \frac{tanh(\beta_c\xi_2/2)}{2\xi_2}] cos(q.\delta_i)\, cos(q.\delta_i - \varphi_\delta) + \frac{sinh(\beta_c\mu)}{2\,cosh(\beta_c\xi_1/2)\,cosh(\beta_c\xi_2/2)} sin(q.\delta_i)\, sin(q.\delta_i - \varphi_\delta)\}$$

for all $i \neq j$. Here, $e^{i\varphi(q)} = \gamma(\vec{q})/|\gamma(\vec{q})|$.

For all the parameters μ and t fixed, we can find the critical temperature and the symmetry of the order parameter by looking for smallest value of β_c for which

$$det(M - I) = 0 \quad (17)$$

As shown in Figure 3, our calculations are consistent with the reported results in Ref. [43]. In this case, our theoretical results indicate the stability of chiral superconductivity is characterized by the breaking of both time-reversal and parity symmetries at any doping level. The chiral d-wave superconducting in the J_1 Heisenberg model on the honeycomb lattice is a spin-singlet $d_{x^2-y^2} \pm id_{xy}$-wave state. Here, the two d-wave states are twofold degenerate due to the sixfold symmetry of the honeycomb lattice. However, these d-wave states have a relative $\pi/2$ phase shift to result in a fully gapped bulk superconducting state.

Following a similar method, we obtain linearized gap equations also for the next nearest-neighbor MF order parameters, $\psi'_{\hat{\delta}}$, and $d'^{\rho}_{\hat{\delta}}$. We find that the $d'^{z}_{\hat{\delta}}$, are coupled with $\psi'_{\hat{\delta}}$, and therefore we can write these linearized gap equations using a stability matrix. To find the critical temperature and the symmetry of the order parameters, we should obtain the eigenvalues of the stability matrices for different channels. Noted that the critical temperature is determined by the largest temperature that at least one of the eigenvalues of different channels be unity [43,44]. In addition, we can obtain the symmetry of the superconducting gap by inserting the eigenvector corresponding to this eigenvalue with the largest temperature in Eq. (13).

We find numerically that the chiral NN-$d_{x^2+y^2} + id_{xy}$-wave pairing is the dominant instability at any doping level. We find no superconducting instability towards the extended-s-wave (es-wave) on the NN pairing of the inter-sublattice component. On the other hand, the NNN-$es + f$-wave exhibits a dominant instability among all the superconducting channels on the NNN pairing of the intra-sublattice component. Figures 4 (a-b) indicate the spatial point symmetry of the es-wave and f-wave order parameters. Indeed, we find, within the mean-field theory, this admixture state of a es-wave state and a f-wave state has a lower energy than other solutions. This mixing is originated from the fact that the spin-triplet component should be aligned to the direction of the quasi Kane-Mele coupling in Eq. (1) [45]. It should be noted that admixture state of the NN-$d + id$- and NNN-$es + f$-wave pairing on the honeycomb lattice is not invariant under the time-reversal symmetry.

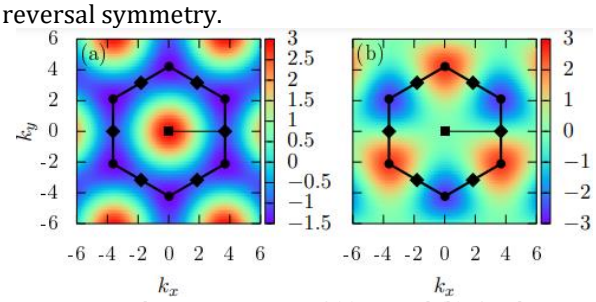

Fig. 4. Spatial point symmetry of (a) es, and (b) f order parameters within FBZ.

4. Conclusion

In summary, we employed a mean-field approach to investigate the possible superconductivities in the twisted WSe_2/WSe_2 homobilayer on the doped moiré Hubbard model. We clearly demonstrated that the admixture of the NN-$d + id$- and NNN-$es + f$-wave pairing was the superconducting ground state at any doping level. Owing to the special lattice structure of the twisted WSe_2/WSe_2 homobilayer, the honeycomb lattice includes the admixture of nearest-neighbor and next-nearest-neighbor pairing components. As abovementioned, the magnitude of the spin-orbit interaction can be well controlled by applying the potential difference between the two layers in the twisted WSe_2, which supports the stability of the spin-triplet superconducting state for different doping levels.

Acknowledgments

M.H.Z. was supported by Grant No. G631021, research deputy of Qom University of Technology.

Conflicts of Interest

The author declares that there is no conflict of interest regarding the publication of this article.

References

[1] Hunt, B., Sanchez-Yamagishi, J.D., Young, A.F., Yankowitz, M., LeRoy, B.J., Watanabe, K., Taniguchi, T., Moon, P., Koshino, M., Jarillo-Herrero, P. and Ashoori, R.C., 2013. Massive Dirac fermions and Hofstadter butterfly in a van der Waals heterostructure. *Science*, *340*(6139), pp.1427-1430.

[2] Dean, C.R., Wang, L., Maher, P., Forsythe, C., Ghahari, F., Gao, Y., Katoch, J., Ishigami, M., Moon, P., Koshino, M. and Taniguchi, T., 2013. Hofstadter's butterfly and the fractal quantum Hall effect in moiré superlattices. *Nature*, *497*(7451), pp.598-602.

[3] Wang, L., Gao, Y., Wen, B., Han, Z., Taniguchi, T., Watanabe, K., Koshino, M., Hone, J. and Dean, C.R., 2015. Evidence for a fractional fractal quantum Hall effect in graphene superlattices. *Science*, *350*(6265), pp.1231-1234.

[4] Spanton, E.M., Zibrov, A.A., Zhou, H., Taniguchi, T., Watanabe, K., Zaletel, M.P. and Young, A.F., 2018. Observation of fractional Chern insulators in a van der Waals heterostructure. *Science*, *360*(6384), pp.62-66.

[5] Cao, Y., Fatemi, V., Demir, A., Fang, S., Tomarken, S.L., Luo, J.Y., Sanchez-Yamagishi, J.D., Watanabe, K., Taniguchi, T., Kaxiras, E. and Ashoori, R.C., 2018. Correlated insulator behaviour at half-filling in magic-angle graphene superlattices. *Nature*, *556*(7699), pp.80-84.

[6] Cao, Y., Fatemi, V., Fang, S., Watanabe, K., Taniguchi, T., Kaxiras, E. and Jarillo-Herrero, P., 2018. Unconventional superconductivity in magic-angle graphene superlattices. *Nature*, *556*(7699), pp.43-50.

[7] Dos Santos, J.L., Peres, N.M.R. and Neto, A.C., 2007. Graphene bilayer with a twist: Electronic structure. *Physical review letters*, *99*(25), p.256802.

[8] Li, G., Luican, A., Lopes dos Santos, J.M.B., Castro Neto, A.H., Reina, A., Kong, J. and Andrei, E.Y., 2010. Observation of Van Hove singularities in twisted graphene layers. *Nature physics*, *6*(2), pp.109-113.

[9] Bistritzer, R. and MacDonald, A.H., 2011. Moiré bands in twisted double-layer graphene. *Proceedings of the National Academy of Sciences*, *108*(30), pp.12233-12237.

[10] Mele, E.J., 2010. Commensuration and interlayer coherence in twisted bilayer graphene. *Physical Review B*, *81*(16), p.161405.

[11] Luican, A., Li, G., Reina, A., Kong, J., Nair, R.R., Novoselov, K.S., Geim, A.K. and Andrei, E.Y., 2011. Single-layer behavior and its breakdown in twisted graphene layers. *Physical review letters*, *106*(12), p.126802.

[12] Dos Santos, J.L., Peres, N.M.R. and Neto, A.C., 2012. Continuum model of the twisted graphene bilayer. *Physical review B*, *86*(15), p.155449.

[13] Moon, P. and Koshino, M., 2012. Energy spectrum and quantum Hall effect in twisted bilayer graphene. *Physical Review B*, *85*(19), p.195458.

[14] Jung, J., Raoux, A., Qiao, Z. and MacDonald, A.H., 2014. Ab initio theory of moiré superlattice bands in layered two-dimensional materials. *Physical Review B*, *89*(20), p.205414.

[15] Wong, D., Wang, Y., Jung, J., Pezzini, S., DaSilva, A.M., Tsai, H.Z., Jung, H.S., Khajeh, R., Kim, Y., Lee, J. and Kahn, S., 2015. Local spectroscopy of moiré-induced electronic structure in gate-tunable twisted bilayer graphene. *Physical Review B*, *92*(15), p.155409.

[16] Fang, S. and Kaxiras, E., 2016. Electronic structure theory of weakly interacting bilayers. *Physical Review B*, *93*(23), p.235153.

[17] Kim, K., DaSilva, A., Huang, S., Fallahazad, B., Larentis, S., Taniguchi, T., Watanabe, K., LeRoy, B.J., MacDonald, A.H. and Tutuc, E., 2017. Tunable moiré bands and strong correlations in small-twist-angle bilayer graphene. *Proceedings of the National Academy of Sciences*, *114*(13), pp.3364-3369.

[18] Nam, N.N. and Koshino, M., 2017. Lattice relaxation and energy band modulation in twisted bilayer graphene. *Physical Review B*, *96*(7), p.075311.

[19] Efimkin, D.K. and MacDonald, A.H., 2018. Helical network model for twisted bilayer graphene. *Physical Review B*, *98*(3), p.035404.

[20] Guinea, F. and Walet, N.R., 2018. Electrostatic effects, band distortions, and superconductivity in twisted graphene bilayers. *Proceedings of the National Academy of Sciences*, *115*(52), pp.13174-13179.

[21] Zou, L., Po, H.C., Vishwanath, A. and Senthil, T., 2018. Band structure of twisted bilayer graphene: Emergent symmetries, commensurate approximants, and Wannier obstructions. *Physical Review B*, *98*(8), p.085435.

[22] Xu, C. and Balents, L., 2018. Topological superconductivity in twisted multilayer graphene. *Physical review letters*, *121*(8), p.087001.

[23] Roy, B. and Juričić, V., 2019. Unconventional superconductivity in nearly flat bands in twisted bilayer graphene. *Physical Review B*, *99*(12), p.121407.

[24] You, Y.Z. and Vishwanath, A., 2019. Superconductivity from valley fluctuations and approximate SO (4) symmetry in a weak coupling theory of twisted bilayer graphene. *npj Quantum Materials*, *4*(1), p.16.

[25] Huang, T., Zhang, L. and Ma, T., 2019. Antiferromagnetically ordered mott insulator and d+ id superconductivity in twisted bilayer graphene: A quantum monte carlo study. *Science Bulletin*, *64*(5), pp.310-314.

[26] Isobe, H., Yuan, N.F. and Fu, L., 2018. Unconventional superconductivity and density waves in twisted bilayer graphene. *Physical Review X*, *8*(4), p.041041.

[27] Wu, F., MacDonald, A.H. and Martin, I., 2018. Theory of phonon-mediated superconductivity in twisted bilayer graphene. *Physical review letters*, *121*(25), p.257001.

[28] Dodaro, J.F., Kivelson, S.A., Schattner, Y., Sun, X.Q. and Wang, C., 2018. Phases of a phenomenological model of twisted bilayer graphene. *Physical Review B*, *98*(7), p.075154.

[29] Po, H.C., Zou, L., Vishwanath, A. and Senthil, T., 2018. Origin of Mott insulating behavior and superconductivity in twisted bilayer graphene. *Physical Review X*, *8*(3), p.031089.

[30] Padhi, B., Setty, C. and Phillips, P.W., 2018. Doped twisted bilayer graphene near magic angles: proximity to Wigner crystallization, not Mott insulation. *Nano letters*, *18*(10), pp.6175-6180.

[31] Yuan, N.F. and Fu, L., 2018. Model for the metal-insulator transition in graphene superlattices and beyond. *Physical Review B*, *98*(4), p.045103.

[32] Chen, G., Jiang, L., Wu, S., Lv, B., Li, H., Watanabe, K., Taniguchi, T., Shi, Z., Zhang, Y. and Wang, F., 2019. Gate-Tunable Mott Insulator in Trilayer Graphene-Boron Nitride Moiré Superlattice. In *APS March Meeting Abstracts* (Vol. 2019, pp. S14-008).

[33] Naik, M.H. and Jain, M., 2018. Ultraflatbands and shear solitons in moiré patterns of twisted bilayer transition metal dichalcogenides. *Physical review letters*, 121(26), p.266401.

[34] Wu, F., Lovorn, T., Tutuc, E., Martin, I. and MacDonald, A.H., 2019. Topological insulators in twisted transition metal dichalcogenide homobilayers. *Physical review letters*, *122*(8), p.086402.

[35] Zhang, Z., Wang, Y., Watanabe, K., Taniguchi, T., Ueno, K., Tutuc, E. and LeRoy, B.J., 2020. Flat bands in twisted bilayer transition metal dichalcogenides. *Nature Physics*, *16*(11), pp.1093-1096.

[36] Wang, L., Shih, E.M., Ghiotto, A., Xian, L., Rhodes, D.A., Tan, C., Claassen, M., Kennes, D.M., Bai, Y., Kim, B. and Watanabe, K., 2020. Correlated electronic phases in twisted bilayer transition metal dichalcogenides. *Nature materials*, *19*(8), pp.861-866.

[37] Muruganandam, V., Sajjan, M. and Kais, S., 2023. Foray into the topology of poly-bi-[8]-annulenylene. *arXiv preprint arXiv:2305.06264*.

[38] Zare, M.H. and Mosadeq, H., 2021. Spin liquid in twisted homobilayers of group-VI dichalcogenides. *Physical Review B*, *104*(11), p.115154.

[39] Zare, M.H., Fazileh, F. and Shahbazi, F., 2013. Zero-temperature phase diagram of the classical Kane-Mele-Heisenberg model. *Physical Review B*, *87*(22), p.224416.

[40] Baskaran, G., Zou, Z. and Anderson, P.W., 1993. The resonating valence bond state and high-Tc superconductivity—a mean field theory. *Solid state communications*, *88*(11-12), pp.853-856.

[41] Lee, P.A., Nagaosa, N. and Wen, X.G., 2006. Doping a Mott insulator: Physics of high-temperature superconductivity. *Reviews of modern physics*, *78*(1), p.17.

[42] Sigrist, M. and Ueda, K., 1991. Phenomenological theory of unconventional superconductivity. *Reviews of Modern physics*, *63*(2), p.239.

[43] Black-Schaffer, A.M. and Doniach, S., 2007. Resonating valence bonds and mean-field d-wave superconductivity in graphite. *Physical Review B*, *75*(13), p.134512.

[44] Zare, M.H., 2020. Competition between spin-singlet and-triplet superconducting states in the doped extended Kitaev-Heisenberg model. *Iranian Journal of Physics Research*, *20*(1), pp.147-155.

[45] Zare, M.H., 2020. Competition between spin-singlet and-triplet superconducting states in the doped extended Kitaev-Heisenberg model. *Iranian Journal of Physics Research*, *20*(1), pp.147-155.